A Brownian Dynamics Study: The Effect of a Membrane Environment on an Electron Transfer System

Dagmar Flöck and Volkhard Helms
Max Planck Institute of Biophysics, Frankfurt, Germany

ABSTRACT During the past few years, three-dimensional crystal structures of many of the important integral membrane proteins responsible for the bioenergetic processes of photosynthesis and respiration have been determined. Moreover, a few crystal structures of protein-protein complexes have become available that characterize the interaction between those membrane proteins and the electron carrier protein cytochrome *c*. Here, we address the association kinetics for binding of cytochrome *c* to cytochrome *c* oxidase (COX) from *Paracoccus denitrificans* by Brownian dynamics simulations. The effects of ionic strength and protein mutations were studied for two different cytochrome *c* species: the positively charged, dipolar horse heart cytochrome *c* and the negatively charged physiological electron transfer partner cytochrome c_{552}. We studied association toward "naked" COX and toward membrane-embedded COX where the membrane is represented as an uncharged DPPC bilayer modeled in atomistic detail. For the nonnatural association toward "naked" COX, the association rates are >100 times larger for horse heart cytochrome *c* than for cytochrome c_{552}. Interestingly, the presence of the lipid bilayer leads to a dramatic decrease of the association rate of horse heart cytochrome *c*, but slightly enhances association of cytochrome c_{552}, leading to very similar association rates of both proteins to membrane-embedded COX. This finding from computational modeling studies may reflect the optimization of surface patches and of the total net charge on electron transfer pairs in nature.

INTRODUCTION

The electron transfer (ET) between cytochrome *c* and cytochrome *c* oxidase (COX) plays a central role in cellular metabolism. The integral membrane protein COX is the terminal enzyme of the respiratory chain in the inner membrane of mitochondria and the cytoplasmic membrane of many bacteria. The water-soluble protein cytochrome *c* functions as electron carrier in the respiratory chain and in photosynthesis. Energy derived from the redox reaction is converted into a proton motive force, which can be used by the cell to drive critical reactions such as synthesis of ATP from ADP.

Protein-protein ET is generally influenced by many structural and dynamic factors. Here, we are not concerned with the details of the ET process itself, but focus on the events leading to the formation of productive ET complexes through rotational and translational diffusion, which are influenced by electrostatic and steric forces. Generally, the kinetics of protein-protein interactions can be divided into diffusion-controlled and reaction-controlled events. Whereas the former are characterized by a very fast reaction after the rate-limiting process of diffusional association, the latter ones catalyze a comparatively slow chemical reaction, usually due to subsequent chemical processes. Preceding any associative protein-protein reaction, an initial diffusional encounter is required, which may limit or at least partially influence the bimolecular rate constant. Therefore, treating the dynamics of associative encounters is of fundamental importance and can well be modeled by Brownian dynamics (BD) simulations for the diffusional motion of larger particles in a continuum solvent environment. Over the past 15 years, BD simulations have become an established technique for computing protein-protein association rates (Northrup et al., 1988; Northrup and Erickson, 1992; Madura et al., 1994; Gabdoulline and Wade, 1998, 2001).

In the absence of systematic forces, the upper limit for the association rate constant of the random search is 7×10^9 $M^{-1}s^{-1}$—dictated by the Smoluchowski equation (Smoluchowski, 1918). Of course, this random collision is far from assuring complex formation, since the relative conformations of the two protein partners add additional constraints, which slow down the reaction by 3–5 orders of magnitude (Berg and von Hippel, 1985; Northrup and Erickson, 1992; Camacho et al., 1999). Association rates have been measured in the range of 10^5–10^9 M^{-1} s^{-1}, where in the fast range the association is enhanced by strong, favorable electrostatic forces (Sheinerman et al., 2000). In contrast to uniformly charged colloidal particles, proteins often carry significant net charges and nonuniform charge distributions. As an example, the net charge of horse heart cytochrome *c* is +7 e and its macromolecular dipole moment 300 Debye (Koppenol and Margoliash, 1982). Consequently, the association is highly dependent on the ionic strength of the solution because the polar interactions between the proteins may be shielded by the solvated ionic charges. On the other hand, the desolvation forces that govern tight binding complexes are

Submitted September 5, 2003, and accepted for publication March 12, 2004.

Address reprint requests to Volkhard Helms, E-mail: Volkhard.Helms@bioinformatik.uni-saarland.de.

Dagmar Flöck's present address is Dept. of Chemistry, University of Rome "La Sapienza", P.le Aldo Moro 5, Rome 00185, Italy.

Volkhard Helms' present address is Centre of Bioinformatics, Saarland University, 66041 Saarbrücken, Germany.

0006-3495/04/07/65/10 $2.00

doi: 10.1529/biophysj.103.035261

independent of the ion concentration, and generally lead to slow binding kinetics.

Experimentally easy-to-control variables are the ionic strength of the solution, which alters the strength of electrostatic interactions, and site-directed mutants, where the importance of individual protein residues on the binding kinetics and thermodynamics can be investigated. The group of Bernd Ludwig (Frankfurt University) has experimentally studied the interaction of COX with cytochrome c_{552} from *Paracoccus denitrificans* and with horse heart cytochrome *c* (Drosou et al., 2002; Maneg et al., 2003). Their kinetic stopped-flow experiments were performed with (fragments of) solubilized COX. The experimental k_{on} values for horse heart cytochrome *c* and wild-type COX, D135N, and N160D mutants are 3.7, 0.3, and 2.8 $\times$ 10^6 $M^{-1}s^{-1}$, respectively (Drosou et al., 2002). For the physiological ET partner cytochrome c_{552}, the k_{on} rates for different ionic strengths of 10, 35, and 200 mM are 4.1, 1.5, and 0.1 $\times$ 10^6 $M^{-1}s^{-1}$, respectively (Maneg et al., 2003). At comparable ionic strength (200 mM vs. 140 mM), the association of cytochrome c_{552} is ~30 times slower than for horse heart cytochrome *c*. This has been explained by its smaller net charge and the less prominent dipolar character (Maneg et al., 2003).

In this study, Brownian dynamics simulations were employed to a), provide a molecular picture for the differential binding properties of the two cytochrome *c* species, and b), to investigate the role of the membrane environment on the binding kinetics of the electron transfer pairs. Since the simulation results should be comparable to the experimental results, our BD simulations were performed with the three-dimensional structures of a soluble cytochrome c_{552} fragment (Harrenga et al., 2000) or the soluble horse heart cytochrome *c*. Although the experimental rates include the diffusional association and the electron transfer step, they should be well comparable to the association rates calculated here because of the rapidity of the ET process (~10^6 s^{-1}). The above listed mutants were chosen because in the experiments of the Ludwig group, D135N showed the largest effect compared to the wild-type, whereas the association rate for N160D stayed in the same order of magnitude. The definition of a successful protein-protein association that leads to the so-called encounter complex is based on a computational docking model (Flöck and Helms, 2002), since no crystal complex structure is available up to now for the pair of cytochrome c_{552}: COX. The encounter complex is stabilized by electrostatic forces as well as by desolvation effects. At this stage, specific short-range interactions do not seem to play an important role (Gabdoulline and Wade, 1999; Janin, 1997; Selzer and Schreiber, 1999). It is an open question in which manner the biological membrane environment influences the protein-protein association and the kinetic behavior of such electron transfer systems. Earlier Brownian dynamics simulations have mostly investigated the interactions of pairs of soluble electron transfer partners, e.g., that of cytochrome *c* with cytochrome *c* peroxidase (Northrup et al., 1988; Castro et al., 1998; Gabdoulline and Wade, 2001) or that of plastocyanin and the membrane-anchored cytochrome *f*, which is a part of the cytochrome b_6/f complex (De Rienzo et al., 2001). Brownian dynamics simulations were recently also reported for the adsorption of hen egg-white lysozyme to a charged solid interface (Ravichandran et al., 2001). Our study seems to be the first study where Brownian dynamics simulations are used to study protein-protein binding in the vicinity of an atomistically modeled membrane.

METHODS

Structures

Coordinates for the two-subunit cytochrome *c* oxidase (COX), determined by Ostermeier et al. (1997) (PDB code 1ar1) to 2.7 Å resolution and for a soluble fragment of cytochrome c_{552} (PDB code 1ql3), determined by Harrenga et al. (2000) to 1.4 Å resolution, both of *P. denitrificans*, were taken from the Protein Data Bank (PDB). Of the four c_{552} molecules contained in the data file, chain B was taken. In the two-subunit COX, each copper atom of the Cu_A center was assigned a charge of +1.5 e (Beinert, 1997; Kannt et al., 1998), giving the two-subunit COX a total charge of −10 e. For horse heart cytochrome *c* (cyt *c*), we used the PDB structure determined by Bushnell et al. (1990) (PDB code 1hrc) at a resolution of 1.9 Å. Assigning neutral histidine residues resulted in a total charge of +7 e for horse heart cytochrome *c* and of −2 e for cytochrome c_{552}.

Computation of forces

Long-range electrostatic forces, calculated using the Poisson-Boltzmann equation, are used to compute the diffusional trajectories of the charged proteins. For each protein, the linear Poisson-Boltzmann equation was solved with the Adaptive Poisson-Boltzmann Solver (APBS) (Baker et al., 2001) or the University of Houston Brownian Dynamics (UHBD) (Davis et al., 1991) package on a 1-Å mesh spacing applying a cubic 161 node grid, whereas for the extended system solely the APBS package was used with same grid size but a 1.55-Å mesh spacing. The solute dielectric constant was set to 2.0, that of the solvent to 78.5, and the calculation was performed for different ionic concentrations. The calculation of the electrostatic grid potentials took ~40 min CPU on a COMPAQ Alpha 667 MHz processor with APBS and 3–4 times longer with UHBD. A comparison of grids for the same system calculated with the two different Poisson-Boltzmann solvers showed satisfactory agreement.

The effective charge method (Gabdoulline and Wade, 1996) was then used to derive charges that represent the external electrostatic potential of the molecule in a uniform dielectric medium (within fitting accuracy). The effective charges ρ_i^{eff} are defined as point charges creating the same potential Φ_i^0 outside the molecule *i* as the partial atomic charges in the inhomogeneous dielectric system

$$\rho^{eff} = \sum_{j=1}^{n} q_j^{eff} \delta(\vec{r} - \vec{r}_j). \quad (1)$$

The *n* effective charges are derived by minimizing a fitting functional, and the integration is performed over the region relevant to intermolecular interaction. To compute forces and torques acting on protein 2(1), the array of effective charges for protein 2(1) is placed on the electrostatic potential

grid of protein 1(2). The method has been successfully applied to a number of systems (Gabdoulline and Wade, 1997, 1998, 2001). Then the electrostatic interaction free energy will be evaluated as the sum of the charge desolvation penalties, where as an estimation, only dipole terms are taken into account, plus the interaction free energy between the effective charges of one molecule with the potential (Φ_i^0) of the other.

The charge desolvation penalties are computed in an approximate fashion that treats the solvation of each charge independently (Elcock et al., 1999). The charge desolvation penalty of protein 1 is taken as the sum of desolvation penalties of each charge of protein 1. The desolvation penalty of each charge is the sum of desolvation penalties due to the low dielectric cavity of each atom of protein 2. Desolvation penalties are computed on a cubic 110 node grid with a 1.5-Å mesh spacing or a 2.5-Å mesh spacing for the extended system.

During the Brownian dynamics simulations, the intermolecular electrostatic interactions were calculated by representing each molecule by a small number of effective charges in a uniform dielectric medium, as described above. This method is as efficient as the test charge method and at the same time provides improved accuracy.

An exclusion volume prohibits van der Waals overlap. The exclusion volume is precalculated on a grid. If a move during the BD simulation would result in van der Waals overlap, the BD step is repeated with different random numbers until it does not overlap. For the grid calculation, a spacing of 1 Å is chosen. Values of 1 are assigned to the interior of the larger protein and 0 outside. The surface-exposed atoms of the smaller protein are listed, and steric overlap is defined to occur when one of the surface-exposed atoms is projected on a grid point with value 1 (Northrup et al., 1987).

Calculation of diffusional bimolecular rate constants

The ensemble flux through a reaction surface of particles, the motion of which is described by the steady-state Smoluchowski diffusion equation, can be obtained as follows

$$\nabla \cdot D(\vec{r})[\nabla - \vec{F}(\vec{r})/k_B T]\rho(\vec{r}) = 0 \tag{2}$$

or

$$\nabla \cdot [-\vec{J}(\vec{r})] = 0, \tag{3}$$

where $\rho(\vec{r})$ is the pair probability density at configuration $\vec{r}$, $\vec{F}(\vec{r})$ is the negative gradient of the intermolecular potential of mean force $U(\vec{r})$, and $D(\vec{r})$ the relative diffusion tensor.

In the BD scheme, trajectories are not terminated when a set of particular reaction criterion is met, but are continued until the surface of an outer sphere of radius c is reached (Northrup et al., 1983). A run will be counted as successful or unsuccessful depending on whether the encounter definitions were fulfilled or not fulfilled during the run. The rate k is then given by (Northrup et al., 1983)

$$k = \frac{k_D(b)\beta}{1 - (1-\beta)k_D(b)/k_D(c)}, \tag{4}$$

where β is determined by the BD simulation as the fraction of the successful runs and $k_D(x)$ is the rate that any particle reaches separation x. The ''start'' sphere surrounding protein 1 typically has a radius of 5–10 Debye lengths plus the molecules' radii, whereas the ''end'' sphere typically has a radius of 15–20 Debye lengths. In the ionic solutions under investigation, the Debye length ranges from a few angstroms to a few nanometers depending on the ionic concentration. In this study we have adapted this scheme for studying membrane-embedded systems (see Figs. 5 and 6).

Simulation technique

Throughout this study the SDA (Simulation of Diffusional Association of proteins) software (Gabdoulline and Wade, 1997, 1998) was used to solve the equations of Brownian motion. The system of two Brownian particles is placed in an initial configuration and moved along a trajectory in accordance with the configuration space distribution function $W(r_i, t)$. The displacements are computed by the Ermak-McCammon algorithm (Ermak and McCammon, 1978):

$$r_i = r_i^0 + \sum_j \frac{\partial D_{ij}^0}{\partial r_j}\Delta t + \sum_j \frac{D_{ij}^0 F_j^0}{kT}\Delta t + R_i(\Delta t). \tag{5}$$

$R_i(\Delta t)$ is a random displacement with Gaussian distribution function fulfilling

$$\langle R_i \rangle = 0 \tag{6}$$

$$\langle R_i(\Delta t) R_j(\Delta t) \rangle = 2D_{ij}^0 \Delta t. \tag{7}$$

To speed up the simulation, hydrodynamic interactions are omitted in this work. In previous studies, the computed encounter rates differed <20% because of this simplification (Antosiewicz and McCammon, 1995; Antosiewicz et al., 1996). As will be shown, electrostatic effects of mutating single residues on either protein have far greater effects on the association rates. The simulated rate constant depends both on radii b and c (see Eq. 4). At distance b the electrostatic forces on the other protein should be isotropic and centrosymmetric. Therefore, as mentioned earlier, b should be chosen in the range of 5–10 Debye lengths. Still, it was observed that even a large decrease of b does not change the order of magnitude of k_{on}. The trajectory truncation distance c was chosen so that making it even larger would not change the computed rates within statistical error. For all simulations, we used $b = 115$ Å and $c = 540$ Å. For cytochrome c, a translational diffusional constant of 0.015 Å^2/ps (Eltis et al., 1991) was assigned. The cytochrome c oxidase translational diffusion constant was calculated applying the Einstein-Stokes relation. For spherical particles in aqueous solution at room temperature, and with an effective hydration radius of ~50 Å for COX, this results in $D = 0.005$ Å^2/ps. Based on these individual diffusion constants, a relative translational diffusion constant of 0.02 Å^2/ps was used and COX was kept fixed during the simulations. A rotational diffusion constant of 4.0×10^{-5} radian^2/ps was assigned to cytochrome c. Since the rotational diffusion constant for spheres goes with the inverse of the hydration radius cubed, the rotational diffusion constant for COX is negligible. Test calculations support this simplification. A variable time step is used that is smaller when the proteins are close to each other and also when the diffusing protein is close to surface c (Gabdoulline and Wade, 1997). For reasons of efficiency, the rotations were performed less frequently than the translations. The rotations are carried out only when the accumulated random component of rotation is 3° at small interprotein separations up to 90° at separations >120 Å. If not denoted differently, these parameters are taken for all simulations.

As structure of the bound complex, the best result of our previously performed docking study (Flöck and Helms, 2002) was used. The coordinates of the complex are required to define the reaction criteria for the Brownian dynamics runs (Gabdoulline and Wade, 1997). The reaction patch is defined by the proximity between one or more intermolecular atom pairs. All interresidue contact pairs that fulfilled the criteria of having a separation distance d_i of less than $d_c = 4.5$ Å in the complex structure were taken for monitoring the resulting association rates. This distance assures a good definition of the protein-protein complex and is the default value used in previous studies with SDA (Gabdoulline and Wade, 1997, 1998). If a shorter separation distance is used, naturally the number of contact pairs is reduced. Therefore, it becomes more and more unlikely that 3–4 contact

pairs reach a close separation distance during the simulation of the diffusional motion. The computed association rate decreases while the statistical error rises. Also such close interresidue distances are rare in modeled protein-protein complexes, especially when they are a result of a computational docking procedure with rigid body structures. On the other hand, increasing the contact distance (and therefore the possible contact pairs) will fail to define the docked complex and overestimate the association rates. Test simulations with different d_c showed that 4.5 Å is the most suitable value to assure for reliable results. Furthermore, to assure for independent contact pairs, the separation distance between the atom pairs is required to be greater than a minimum distance $d_{min} = 7.0$ Å.

For wild-type COX of *P. denitrificans* and horse heart cytochrome *c*, the following interresidue pairs served for the definition of reaction criteria:

Asp^{156}:OD2-Lys^{79}:NZ	Ala^{259}:O-Lys^{73}:NZ	Ser^{124}B:OG-Lys^{86}:NZ
Asp^{135}B:OD2-Lys^{86}:NZ	Asp^{135}B:OD1-Lys^{86}:NZ	Tyr^{122}B:OH-Gly^{84}:O.

The distance between them was monitored throughout the runs.

For the mutant D135N of COX from *P.* and horse heart cytochrome *c*, the following interresidue pairs were used:

Asn^{135}B:OD1-Lys^{86}:NZ	Asn^{135}B:OD1-Lys^{86}:NZ	Asn^{135}B:OD1-Lys^{86}:NZ
Asn^{135}B:OD1-Lys^{86}:NZ	Tyr^{122}B:OH-Gly^{84}:O	

These are the same pairs as for wild-type, except that due to the D135N mutation, two atom pairs between Asp^{135} and Lys^{86} were removed from the list. Instead, the separation distance between one atom pair between Asn^{135} and Lys^{86} was monitored. A set of test simulations for wild-type COX using the contact pairs of D135N showed only small decreases in the association rates by a factor of 3. Therefore, the small k_{on} rates computed for D135N (see below) indeed reflect the influence of the protein mutation on k_{on} and are not simply due to a different definition of contact pairs.

For wild-type COX and its physiological ET partner cytochrome c_{552}, the following interresidue pairs were used:

Asp^{156}:OD2-Asn^{45}:ND2	Asp^{156}:OD2-Lys^{77}:NZ	Gln^{254}:OE1-Asn^{68}:ND2
Asp^{257}:OD1-Lys^{70}:NZ	Asp^{257}:OD2-Lys^{70}:NZ	Ala^{259}:O-Asn^{68}:ND2
Tyr^{122}:OH-Lys^{13}:N	Asp^{135}:OD2-Lys^{15}:NZ	Thr^{177}:O-Ala^{81}:N
ALA^{251}:O-Lys^{9}:NZ	Tyr^{122}:OH-Gly^{12}:O	Tyr^{122}:OH-Lys^{13}:O

For each system, 4 × 4000 runs (with four different random number seeds) were performed, and the results were averaged over all simulated rates. The CPU time necessary for 16,000 runs is 32–48 h on a COMPAQ Alpha 667 MHz processor.

Setup of membrane-embedded system

To study the influence of a membrane environment on the dynamics of cytochrome *c* and on its interaction with cytochrome *c* oxidase, a bilayer had to be constructed around the integral membrane protein COX. Based on the geometry of the docked complex, the binding patch for cytochrome *c* on the COX surface is only ~1 nm away from the membrane surface, which equals ~1 Debye length. The membrane should not simply be considered as a geometrical perturbation because, at such close distances, atomic details may become very relevant. Consequently, the membrane was represented in atomic detail as well. The construction of a lipid bilayer surrounding followed a protocol developed in B. Roux's group (Woolf and Roux, 1994, 1996) with slight modifications. The strategy consists of randomly selecting lipids from a prehydrated and preequilibrated set, scattering the lipids around the protein and reducing the number of overlaps by systematic rigid-body rotations and translations. To surround the protein by a complete lipid environment, the dimensions of the system in the *x, y* plane were set at 75 Å × 75 Å corresponding to an area of 5625 $Å^2$. Since the average cross-sectional area of a DMPC/DPPC molecule is 64 $Å^2$ (Gennis, 1989; Nagle, 1993), the appropriate number of lipids was determined to 51 for the upper bilayer and 50 for the lower bilayer. The DPPC polar heads were first represented by large spheres with the same cross section to determine the initial position of each lipid. Molecular dynamics and energy minimization with adequate boundary conditions were performed while constraining the spheres at $z = +19$ Å and $z = -19$ Å for the upper and lower layers, respectively. These spheres were then substituted by full DPPC lipids randomly chosen from a library of 2000 prehydrated and preequilibrated phospholipids (Venable et al., 1993). Systematic rigid body rotations of the lipids around the *z* axis and translations in the *x, y* plane were performed to remove steric clashes and unfavorable atomic contacts, followed by an energy minimization to optimize the configuration. Next a preequilibrated water box of appropriate dimension was overlayed with the system and the resulting system was refined by energy minimization. Fig. 1 shows this system in atomic detail. The DPPC lipids exhibit a zwitterionic nature but are overall neutral. The electrostatic properties of this structure are studied in the Results section. For the Brownian dynamics simulations, the previously constructed membrane-embedded protein system (''central unit'') was expanded with pure lipid bilayers of the same unit length 75 Å that were placed around the central unit. The total system has dimensions of 225 Å and contains more than 200,000 atoms (including hydrogen atoms).

RESULTS

Electrostatic results

The potential isocontours of the ''central unit'' for membrane-embedded COX (Fig. 2, *right*) at +1 *kT*/e (*blue*) and −1 *kT*/e (*red*) are compared to those for ''naked'' COX (*left*). Separately marked is Trp^{121} of COX, the electron entry site on the COX binding interface (Witt et al., 1998a,b). The most obvious feature is the overall negative electrostatic potential of the oxidase as well as the positive electrostatic potential of the lipids. Consequently, the positively charged lysine residues on the cytochrome *c* surface will be less

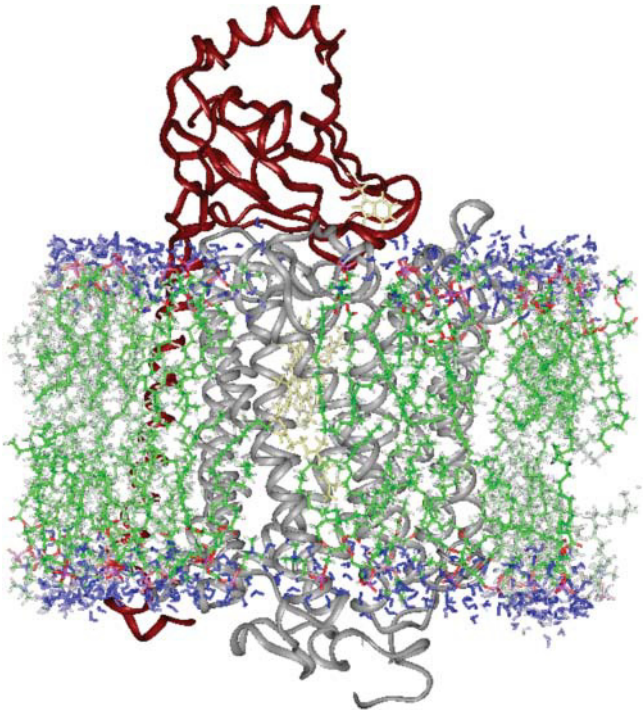

FIGURE 1 Partly solvated lipid bilayer (*green*) around cytochrome *c* oxidase (*gray* plus *red ribbon*). The electron entry site of COX is shown in yellow.

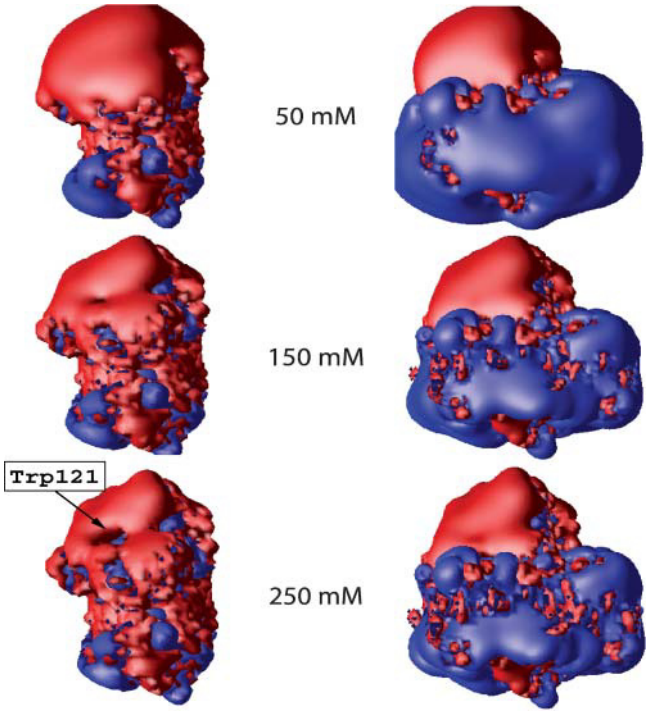

FIGURE 2 Potential isocontours shown at + 1 *kT*/e (blue) and − 1 *kT*/e (*red*) of COX alone (*left*) and of the central unit of COX surrounded by lipid bilayer (*right*). The electron entry site Trp^{121} is less exposed when COX is membrane-embedded.

attracted the more the oxidase charges are shielded by ions in the bulk solution.

Wild-type, D135N, and N160D COX of *P. denitrificans* and horse heart cytochrome *c* (140 mM)

In Fig. 3 the simulated k_{on} rates for the pair of COX and horse heart cytochrome *c* are shown versus the root mean-square distance of the defined contact pairs. Naturally, the rates are highest when only one contact criterion has to be met (*top line*) and decrease when more contacts have to be fulfilled simultaneously (from *top* to *bottom*) (see Gabdoulline and Wade, 1997). Also, a strong dependence of the rates on the separation distance of the contact pairs can be seen: they drop markedly when the separation distance between the interresidue pairs comes to a few angstroms. For comparison, the experimentally measured value is indicated by a horizontal dashed-dotted line. The simulated rates for three contact pairs are closest to the experimental data. Still, even when tight contact separation distances of 5.0–5.5 Å are required, association rates are 10–100-fold overestimated by the simulation. In this figure we also show the standard deviation of the 4 × 4000 runs. These errors are typical for all simulations performed in this work. As for wild-type, the experimental result for the mutant D135N is best matched when three contact pairs are taken to define the encounter complex and a contact separation distance of <5.5 Å is satisfied. Still, the experimentally measured value is overestimated by ~1 order of magnitude. For the N160D mutant, the same interresidue pairs were monitored throughout the BD runs as for wild-type since they are not affected by the N160D mutation. As before, the definition of the encounter complex can best be realized by three contact pairs. The association rate for these three contact pairs and a separation distance of <5.5 Å overestimates the experimental value up to 150-fold. In good quantitative agreement with the experimental data, N160D is close to the wild-type data whereas D135N association is markedly slower. Since a charged residue (Asp, D) is substituted by a polar, uncharged residue (Asn, N) and vice versa, both mutations influence the electrostatic field. The altered electrostatic properties of COX are reflected in the observed rates, especially when the affected residues play a key role in the association process. Such relative trends can usually very well be reproduced by Brownian dynamics simulations even if the absolute rates are not in perfect agreement with experiment (Gabdoulline and Wade, 1998).

Wild-type COX and soluble fragment of cytochrome c_{552} of *P. denitrificans* (10, 35, and 200 mM)

The simulated association rates for 10, 35, and 200 mM ionic strength are presented in Fig. 4. As for horse heart

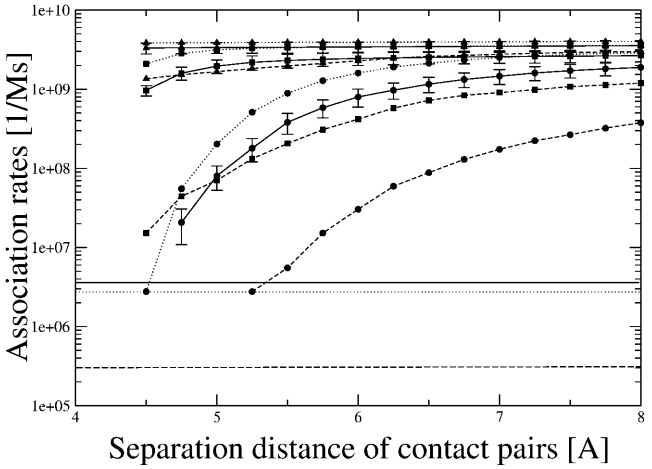

FIGURE 3 Simulated association rates for wild-type COX (*solid line*), D135N (*dashed line*), N160D (*dotted line*), and horse heart cytochrome *c* at 140 mM. k_{on} is shown for various reaction pair distances for one (*triangles*), two (*squares*) and three (*circles*) interresidue pairs. The experimentally measured values are included in the graph and depicted by the corresponding horizontal lines. The error bars show the statistical error of the simulation. The effect of the mutations on the association rate is qualitatively reproduced by the BD simulation.

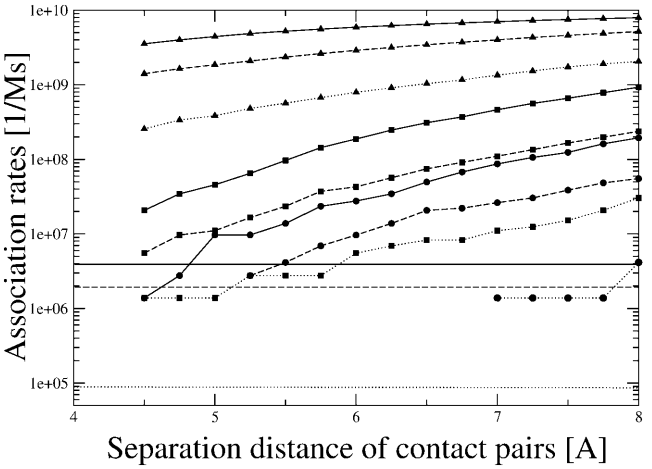

FIGURE 4 Simulated association rates for COX and its physiological ET partner cytochrome c_{552} at 10 mM (*solid line*), 35 mM (*dashed line*), and 200 mM (*dotted line*). k_{on} is shown in relationship to the reaction pair distance for one (*triangles*), two (*squares*) and three (*circles*) interresidue pairs. The experimentally measured values are included in the graph and are depicted by the corresponding horizontal lines. The effect of the ionic strength of the solution on the association rates are qualitatively reproduced by the BD simulation.

cytochrome *c*, the simulated association rates are overestimated compared to the experimental data. For three contact pairs and a separation distance of 5.5 Å between the interresidue pairs, simulated k_{on} values are higher by up to one order of magnitude. Similar to the experimental rates, a), the simulated k_{on} rates at comparable ionic strength (200 mM vs. 140 mM) are much lower for cyt c_{552} than for horse heart cyt *c*, and b), the experimental data the association becomes smaller as the ionic strength of the surrounding solution rises.

Association rates for membrane-embedded systems

Simulations with membrane-embedded cytochrome *c* oxidase were performed with a modified setup. Trajectories were now started only at the upper hemisphere (see Fig. 5 for a scheme of the modified setup). The algorithm was changed in the way that the randomly chosen starting positions are accepted only if they lie on the protein-protein interaction side of the system. Also a minimum distance to the membrane of 20 Å is required so that the diffusional simulation of the smaller particle is not started too close to the membrane. Note that diffusing particles can still easily pass over to the other side of the membrane and may leave the outer sphere (not shown) everywhere. The new setup was tested against the standard setup with a BD simulation for the pair of ''naked'' cytochrome *c* oxidase and horse heart cytochrome *c*. A comparison of the simulated rates is shown in Fig. 6 and shows excellent agreement.

In Fig. 7 the calculated association rates for membrane-embedded COX and horse heart cytochrome *c* are shown. A direct comparison of k_{on} rates computed with three contact pairs for COX within and without the lipid bilayer is shown in Fig. 8. The computed association rates for the membrane-embedded system are two orders of magnitude lower than the computed rates for ''naked'' COX. The effect can be attributed to the different electrostatic potential (see above). The graph additionally shows a comparison of the calculated k_{on} rates for the membrane system using electrostatic potential grids computed either with UHBD or APBS. Both sets of calculations give very similar results.

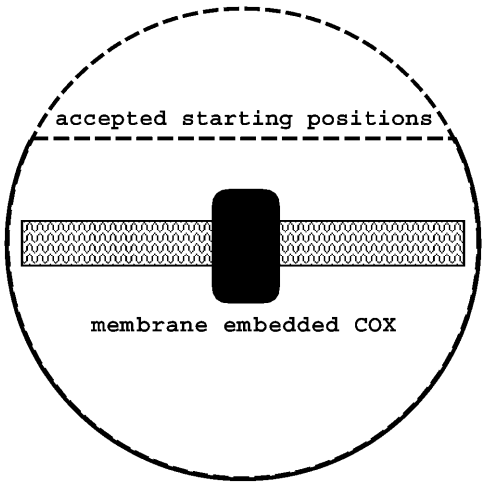

FIGURE 5 Scheme of modified setup for Brownian dynamics simulations. Trajectories are started exclusively at the upper hemisphere (*dashed line*).

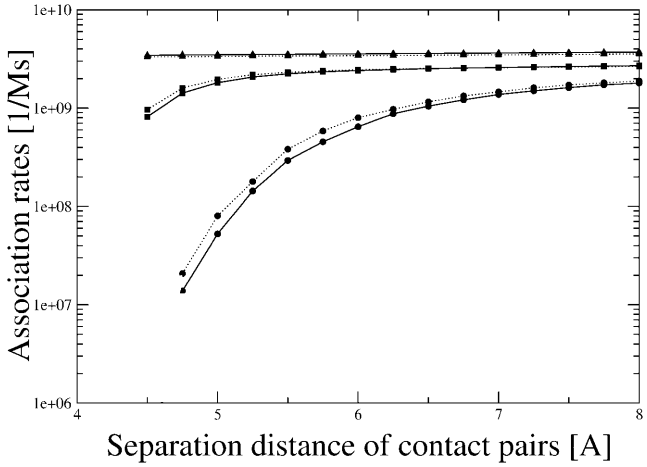

FIGURE 6 Test simulation of COX and horse heart cytochrome *c* at 140 mM for original (*dotted lines*) and special setup of SDA (*solid lines*), which was modified to account for the inclusion of the membrane environment. The deviation lies well within the statistical error.

Fig. 7 also shows the k_{on} rates calculated from BD simulations of membrane-embedded COX and its physiological electron transfer partner cytochrome c_{552}. The comparison reveals that the computed rates for horse heart cyt *c* and cyt c_{552} are now in the same range. Whereas the association to ''naked'' COX was much faster for horse heart cyt *c*, the lipid environment now favors the association of cyt c_{552}.

Fig. 8 compares the results of COX without and within the lipid bilayer. In contrast to the system of COX and horse heart cytochrome *c*, the k_{on} rates for the membrane embedded COX:cyt c_{552} are slightly higher than for ''naked'' COX for contact distances up to 11.0 Å. This can be explained by the fact that compared to horse heart cyt *c*, cytochrome c_{552} has a considerably lower net charge of opposite (negative)

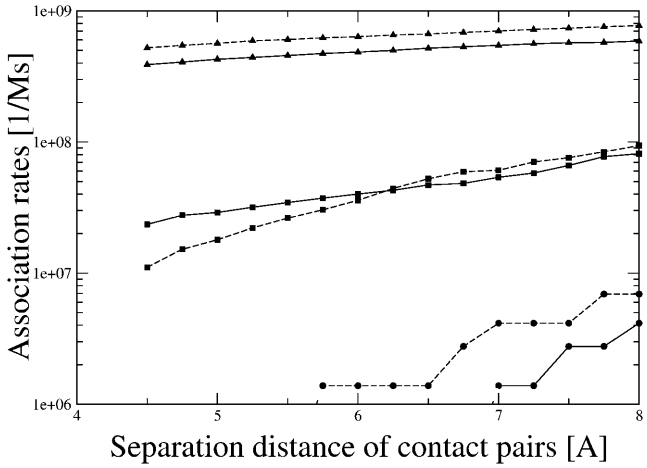

FIGURE 7 Simulated association rates for membrane embedded COX and horse heart cytochrome *c* at 140 mM (*solid line*) as well as membrane embedded COX and cytochrome c_{552} at 200 mM (*dashed line*).

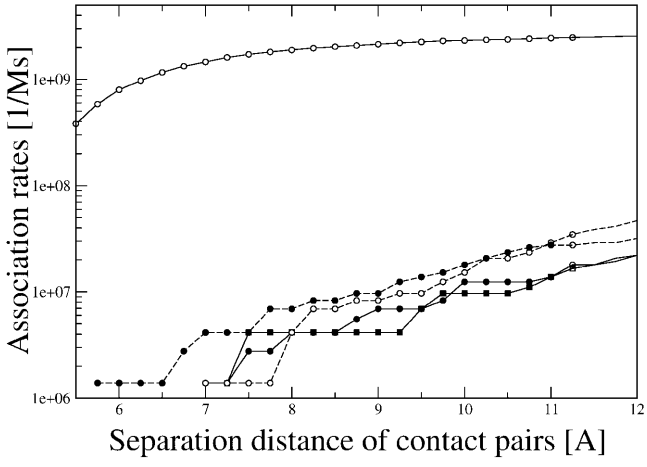

FIGURE 8 Comparison of simulated association rates for COX without (*solid line*, *open circles*) and within (*solid line*, *solid circles*, and *solid squares*) the membrane environment and horse heart cytochrome *c* at 140 mM. For comparison, the latter simulations were performed with electrostatic grids calculated either by UHBD (*solid squares*) or by APBS (*solid circles*). In the same manner, a comparison of computed association rates for three contact pairs of membrane-embedded COX (*dashed line*, *solid circles*) and ''naked'' COX (*dashed line*, *open circles*) with its physiological ET partner cytochrome c_{552} is shown. Remarkably, the lipid bilayer influences the association rates of the two systems differently.

sign. The physiological electron transfer partner cyt c_{552} also shows a significantly reduced bipolar character. Because the electrostatic steering effect is much smaller for the diffusing reacting partner, the change of the electrostatic potential introduced by the bilayer does not diminish the association rate.

One advantage of computational modeling is that it allows dissection of the underlying energetic components governing the complicated association kinetics of complex systems. Fig. 9 shows the association rates for membrane-embedded COX using three contact pairs when the system charges are turned to zero, whereas Fig. 10 shows the association kinetics when either the membrane charges or the COX charges are turned to zero. For both systems (Fig. 9), switching off electrostatics increases the simulated k_{on} rates. This demonstrates that it is electrostatically unfavorable for cyt *c* to squeeze into the binding interface in close vicinity of the lipid bilayer. The results for cytochrome *c* shown in Fig. 10 reveal competing roles of the attractive COX binding patch and the unfavorably charged membrane surface. The results for cytochrome c_{552} are less intuitive. In both cases, either switching off the membrane charges or the COX charges, the association rates are significantly increased. This different behavior is discussed in the following section.

DISCUSSION

Brownian dynamics simulations allowing the computing of kinetic association rates of two rigid-body proteins that

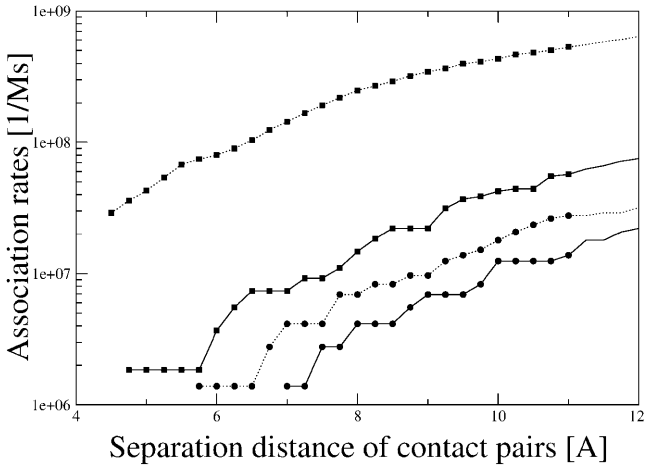

FIGURE 9 Comparison of association kinetics for binding of cytochrome *c* (*solid lines*) and cytochrome c_{552} (*dotted lines*) to the membrane-embedded COX using three contact pairs when the system charges are turned to zero (*solid squares*) to the original association rates with full electrostatics (*solid circles*).

interact electrostatically and sterically were employed to investigate the effect of a membrane environment on the association kinetics of an electron transfer pair from the respiratory chain, cytochrome *c*, and cytochrome *c* oxidase.

Although the model allowed quite accurate predictions of relative association rates for mutated proteins and different ionic strengths, the quantitative prediction of real association rates still seems difficult to obtain with such simplified models. In particular, the kinetic on-rates for association to ''naked'' cytochrome *c* oxidase are systematically computed 10–100 times higher than measured in experiment. It is hard to exactly quantify the amount of overestimation because it is

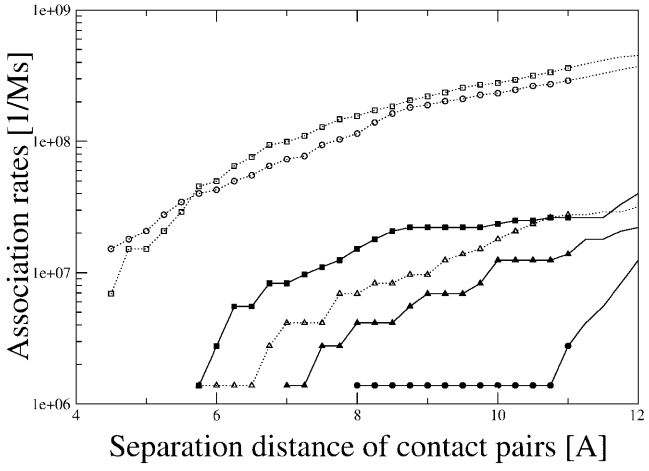

FIGURE 10 Computed association kinetics for binding of cytochrome *c* (*solid lines*, *solid symbols*) and cytochrome c_{552} (*dotted lines*, *open symbols*) to the membrane-embedded COX using three contact pairs when either the membrane charges (*squares*) or the COX charges (*circles*) are turned to zero. For comparison, the association rates calculated with full electrostatics are also included (*triangles*).

unclear where to define the encounter complex. Previous BD simulation studies performed with UHBD and SDA (Gabdoulline and Wade, 1998; Elcock et al., 1999) have shown similar overestimations of the association rates. Still, the improved treatment of desolvation effects (Elcock et al., 1999), which is applied here, has generally been able to improve the matching between experimental and computational results.

First we like to discuss the validity of the computationally docked complex as a basis for BD simulations. After the computations of this study were completed, an NMR study (Wienk et al., 2003) characterized residues at the binding interface between COX and cyt c_{552} by measuring chemical shifts of cyt c_{552} residues between the free form and in the complex with COX. Some residues supposed to lie at the binding interface according to our computational docking complex (Flöck and Helms, 2002) did not show noticeable chemical shifts. Of the residues used in this study for definition of the encounter complex, only Lys^{70} and Ala^{81} show large chemical shifts. This is at first surprising because, e.g., Lys^{13} and Lys^{77} are located in the immediate vicinity of the heme group of cyt c_{552}. However, a recent crystal structure of a cytochrome c_2:reaction center complex from *Rhodobacter sphaeroides* (Axelrod et al., 2002) showed that ion pairs at the protein-protein interface did not establish direct contacts but remained separated by 5–6 Å. This can be rationalized by assuming an unfavorable desolvation energy for formation of the ion pairs. It is therefore well possible that this principle also applies to the complex of COX and cyt c_{552}. Commonly, protein-protein association is regarded as a two-step process (Schreiber, 2002; Camacho and Vajda, 2002). The measured chemical shifts would then occur in the second step when the tightly bound complex is assembled. Electrostatic steering, on the other hand, as reflected by the effect of charge mutations that showed a significant effect on the k_{on} rates deduced from the onset of the electron transfer (Witt et al., 1998a,b), is more important for the first step (formation of an encounter complex). Therefore, the docking model appears to be a reasonable choice for definition of the encounter complex that is not equivalent to the tightly bound complex studied by NMR experiments under equilibrium conditions.

Second, the overestimation of the computed rates might very well be due to the kinetic behavior of these electron transfer systems. Possibly, there is a high free-energy barrier between the encounter and the bound complex as has been proposed for some protein-protein complexes (Selzer and Schreiber, 2001). Therefore, the postencounter steps of association, which could not be included in our simulations, could slow down the real association rates significantly. Evidence for this kinetic scheme also comes from the above-mentioned NMR study of the COX:cyt *c* complex formation (Wienk et al., 2003). A possible computational approach would be to combine Brownian dynamics simulations for association up to a certain distance of, e.g., 10 Å with steered

molecular dynamics simulations to describe the final binding process where molecular details (e.g., interfacing water molecules) and flexibility of residues at the interface would become important.

Finally, we mention again that experimental k_{on} rates are conducted with solubilized COX, and this might be a possible explanation for the discrepancy between experimental and simulated values as well. In the experimental setup, the transmembrane part of COX is surrounded by a detergent belt of dodecyl maltoside molecules, which could change the electrostatic properties of the system and therefore also the association rate. The detergent belt around cytochrome *c* oxidase molecules could either simply mean excluded volume or may specifically interact with the diffusing cytochrome *c* particles. Here, it would be helpful to know the exact protein/lipid content to set up simulations exactly mimicking the experimental conditions.

The most interesting finding of this study is the differential effect of the membrane environment on the association kinetics of cytochrome c_{552} versus cytochrome *c* to cytochrome *c* oxidase. For cytochrome *c* the k_{on} rates are 100–1000 times slower depending on the defined reaction distance when the membrane environment is included. On the other hand, no noticeable effect is seen for the binding of cytochrome c_{552}. Besides its electrostatic role, the membrane may simply act as a steric barrier because a), the binding site of COX is only ~10 Å above the bilayer, and b), the contour plots of the electrostatic potential give evidence that the hydrophobic patch of the COX electron entry side, which is surrounded by acidic side chains, loses its exposition when the enzyme is surrounded by a membrane.

Even though the net charge of single DPPC lipids is zero, the calculation of the electrostatic potential of the membrane-embedded protein system (see Fig. 2) revealed that the membrane is attractive to negatively charged particles. One would therefore expect that it has a stronger effect for horse heart cytochrome *c* that has a total positive charge versus the negatively charged cytochrome c_{552}. But the effects may be more subtle because the cytochromes are dipolar particles, and it is mostly the positively charged lysine side chains at the binding interface that will be repelled from the membrane surface. On the other hand, both cytochromes were predicted to bind in different orientations (Flöck and Helms, 2002), and the membrane influence may act differently on both orientations. Computational modeling allows the dissection of such situations. In a first set of test calculations, the electrostatic charges of the membrane were switched off so that only the steric presence (exclusion grid) is felt by the diffusing cytochrome particles. Interestingly, the association rates of both cytochrome c_{552} and cytochrome *c* increase significantly. When switching off only the charges of COX, cytochrome c_{552} again binds faster, whereas cytochrome *c* binding is significantly decreased. This indicates a), that it is only the favorable electrostatic attraction of the binding patch on COX that brings horse heart cytochrome *c* in the vicinity of the membrane surface, whereas b), the effects must be more subtle in the case of cytochrome c_{552} because binding of cytochrome c_{552} to COX was equally fast with and without membrane. Probably due to a competition between attractive binding patch on COX and attraction by the membrane surface, the binding kinetics increases when either COX or membrane charges are switched off. We suggest that this delicate balance of competing attractions is optimized for the association of the physiological pair of cytochrome c_{552} and COX. Also, one should take into account that the protein-protein association of cytochrome *c* and COX is of transient nature and solely has the purpose of mediating electron transfer between both proteins. Therefore, it may functionally be advantageous not to create a ''too comfortable'' binding region for cytochrome *c*. It makes sense to assume that oxidized cytochrome *c* after ET will be even less strongly bound than reduced cytochrome *c*.

There is now good experimental evidence (Schägger and Pfeiffer, 2001; Schägger, 2002) that the enzymes of the respiratory chain and of the photosynthetic units build supercomplexes and their stoichiometry could widely affect the electron transfer. The computational methods presented in this work are well suited to investigate these nanosystems. Once the supercomplexes are computationally docked, the electrostatic properties could be studied, and Brownian dynamics simulations could be performed. Additionally, the diffusional motion of many cytochrome *c* particles can be incorporated in computationally more demanding simulations. Theoretical investigations of such multi-particle systems are just beginning to appear (Gorba and Helms, 2003) and will ultimately deepen the understanding of such multi-molecular systems.

The authors are grateful to R. C. Wade for providing the SDA package and to R. Gabdoulline for extensive help with the package. The authors also thank N. Baker for providing the APBS package and help with its usage, E. Olkhova for cooperation on the membrane construction, and B. Ludwig for sharing data before publication and for valuable discussions.

This work was financially supported by Sonderforschungsbereich 472 (Teilprojekt 23) of the Deutsche Forschungsgemeinschaft.

REFERENCES

Antosiewicz, J., J. M. Briggs, and J. A. McCammon. 1996. Orientational steering in enzyme-substrate association: ionic strength dependence of hydrodynamic torque effects. *Eur. Biophys. J.* 24:137–141.

Antosiewicz, J., and J. A. McCammon. 1995. Electrostatic and hydrodynamic orientational steering effects in enzyme-substrate association. *Biophys. J.* 69:57–65.

Axelrod, H. L., E. C. Abresch, M. Y. Okamura, A. P. Yeh, D. C. Rees, and G. Feher. 2002. X-ray structure determination of the cytochrome-c(2):reaction center electron transfer complex from *Rhodobacter* sphaeroides. *J. Mol. Biol.* 319:501–515.

Baker, N. A., D. Sept, S. Joseph, M. J. Holst, and J. A. McCammon. 2001. Electrostatics of nanosystems: application to microtubules and the ribosome. *Proc. Natl. Acad. Sci. USA.* 98:10037–10041.

Beinert, H. 1997. Copper A of cytochrome *c* oxidase, a novel long-embattled, biological electron-transfer site. *Eur. J. Biochem.* 245: 521–532.

Berg, O. G., and P. H. von Hippel. 1985. Diffusion-controlled macromolecular interactions. *Annu. Rev. Biophys. Biophys. Chem.* 14: 131–160.

Bushnell, G. W., G. V. Louie, and G. D. Brayer. 1990. High-resolution three-dimensional structure of horse heart cytochrome c. *J. Mol. Biol.* 214:585–595.

Camacho, C. J., and S. Vajda. 2002. Protein-protein association kinetics and protein docking. *Curr. Opin. Struct. Biol.* 12:36–40.

Camacho, C. J., Z. Weng, S. Vajda, and C. DeLisi. 1999. Free energy landscapes of encounter complexes in protein-protein association. *Biophys. J.* 76:1166–1178.

Castro, G., C. A. Boswell, and S. H. Northrup. 1998. Dynamics of protein-protein docking: cytochrome *c* and cytochrome *c* peroxidase revisited. *J. Biomol. Struct. Dyn.* 16:413–424.

Davis, M. E., J. D. Madura, B. A. Luty, and J. A. McCammon. 1991. Electrostatic and diffusion of molecules in solution: simulations with the University of Houston Brownian Dynamics Program. *Comput. Phys. Comm.* 62:187–197.

Drosou, V., F. Malatesta, and B. Ludwig. 2002. Mutations in the docking site for cytochrome *c* on the *Paracoccus* heme aa_3 oxidase: electron entry and kinetic phases of the reaction. *Eur. J. Biochem.* 269:2980–2988.

Elcock, A. H., R. R. Gabdoulline, R. C. Wade, and J. A. McCammon. 1999. Computer simulation of protein-protein association kinetics: acetylcholinesterase-fasciculin. *J. Mol. Biol.* 291:149–162.

Eltis, L. D., R. E. Herbert, P. D. Barker, A. G. Mauk, and S. H. Northrup. 1991. Reduction of horse heart ferricytochrome *c* by bovine liver ferrocytochrome *b*5. *Biochemistry.* 30:3663–3674.

Ermak, D. L., and J. A. McCammon. 1978. Brownian dynamics with hydrodynamic interactions. *J. Chem. Phys.* 69:1352–1360.

Flöck, D., and V. Helms. 2002. Protein-protein docking of electron transfer complexes: cytochrome *c* oxidase and cytochrome *c*. *Proteins.* 47:75–85.

Gabdoulline, R. R., and R. C. Wade. 1996. Effective charges for macromolecules in solvent. *J. Phys. Chem.* 100:3868–3878.

Gabdoulline, R. R., and R. C. Wade. 1997. Simulation of diffusional association of barnase and barstar. *Biophys. J.* 72:1917–1929.

Gabdoulline, R. R., and R. C. Wade. 1998. Brownian dynamics simulation of protein-protein diffusional encounter. *Methods.* 14:329–341.

Gabdoulline, R. R., and R. C. Wade. 1999. On the protein-protein diffusional encounter complex. *J. Mol. Recognit.* 12:226–234.

Gabdoulline, R. R., and R. C. Wade. 2001. Protein-protein association: investigation of factors influencing association rates by Brownian Dynamics simulation. *J. Mol. Biol.* 306:1139–1155.

Gennis, R. B. 1989. Biomembranes Molecular Structure and Function. Springer-Verlag, New York.

Gorba, C., and V. Helms. 2003. Diffusional dynamics of cytochrome *c* molecules in the presence of a charged surface. *Soft Materials.* 1:413–424.

Harrenga, A., B. Reincke, H. Ruterjans, B. Ludwig, and H. Michel. 2000. Structure of the soluble domain c(552) from *Paracoccus denitrificans* in the oxidized and reduced states. *J. Mol. Biol.* 295:667–678.

Janin, J. 1997. The kinetics of protein-protein recognition. *Proteins.* 28:153–161.

Kannt, A., C. R. Lancaster, and H. Michel. 1998. The coupling of electron transfer and proton translocation: electrostatic calculations on *Paracoccus denitrificans* cytochrome *c* oxidase. *Biophys. J.* 74:708–721.

Koppenol, W. H., and E. Margoliash. 1982. The asymmetric distribution of charges on the surface of horse cytochrome c. *J. Biol. Chem.* 257:4426–4437.

Madura, J. D., J. M. Briggs, R. Wade, B. A. Luty, A. Ilin, J. Antosiewicz, M. K. Gilson, B. Bagheri, L. Ridgway Scott, and J. A. McCammon. 1994. Biological applications of electrostatics calculations and Brownian dynamics simulations. *Rev. Comput. Chem.* 5:229–267.

Maneg, O., B. Ludwig, and R. Malatesta. 2003. Different interaction modes of two cytochrome *c* oxidase soluble CuA fragments with their substrates. *J. Biol. Chem.* 278:46734–46740.

Nagle, J. F. 1993. Area/lipid of bilayers from NMR. *Biophys. J.* 64:1476–1481.

Northrup, S. H., S. A. Allison, and J. A. McCammon. 1983. Brownian dynamics simulation of diffusion-influenced bimolecular reactions. *J. Chem. Phys.* 80:1517–1524.

Northrup, S. H., J. O. Boles, and J. C. Reynolds. 1988. Brownian dynamics of cytochrome *c* and cytochrome *c* peroxidase association. *Science.* 241:67–70.

Northrup, S. H., J. O. Boles, and J. C. L. Reynolds. 1987. Electrostatic effects in the Brownian dynamics of association and orientation of heme proteins. *J. Phys. Chem.* 91:5991–5998.

Northrup, S. H., and H. P. Erickson. 1992. Kinetics of protein-protein association explained by Brownian dynamics computer simulation. *Proc. Natl. Acad. Sci. USA.* 89:3338–3342.

Ostermeier, C., A. Harrenga, U. Ermler, and H. Michel. 1997. Structure at 2.7 Å resolution of the *Paracoccus denitrificans* two-subunit cytochrome *c* oxidase complexed with an antibody F-V fragment. *Proc. Natl. Acad. Sci. USA.* 94:10547–10553.

Ravichandran, S., J. D. Madura, and J. Talbot. 2001. A Brownian dynamics study of the initial stages of hen egg-white lysozyme adsorption at a solid interface. *J. Phys. Chem.* 105:3610–3613.

De Rienzo, F., R. R. Gabdoulline, M. C. Menziani, P. G. De Benedetti, and R. C. Wade. 2001. Electrostatic analysis and Brownian dynamics simulation of the association of plastocyanin and cytochrome *f*. *Biophys. J.* 81:3090–3104.

Schägger, H. 2002. Respiratory chain supercomplexes of mitochondria and bacteria. *Biochim. Biophys. Acta.* 1555:154–159.

Schägger, H., and K. Pfeiffer. 2001. The ratio of oxidative phosphorylation complexes I-V in bovine heart mitochondria and the composition of respiratory chain supercomplexes. *J. Biol. Chem.* 276:37861–37867.

Schreiber, G. 2002. Kinetic studies of protein-protein interactions. *Curr. Opin. Struct. Biol.* 12:41–47.

Selzer, T., and G. Schreiber. 1999. Predicting the rate enhancement of protein complex formation from the electrostatic energy of interaction. *J. Mol. Biol.* 287:409–419.

Selzer, T., and G. Schreiber. 2001. New insight into the mechanism of protein-protein association. *Proteins.* 45:190–198.

Sheinerman, S. H., R. Norel, and B. Honig. 2000. Electrostatic aspects of protein-protein interactions. *Curr. Opin. Struct. Biol.* 10:153–159.

Smoluchowski, M. V. 1918. Towards a mathematical theory of the coagulation kinetics of colloidal solutions. *Z. Phys. Chem.* 92:129–168.

Venable, R. M., Y. Zhang, B. J. Hardy, and R. W. Pastor. 1993. Molecular dynamics simulations of a lipid bilayer and of hexadecane: an investigation of membrane fluidity. *Science.* 262:223–226.

Wienk, H., O. Maneg, C. Lücke, P. Pristovšek, F. Löhr, B. Ludwig, and H. Rüterjans. 2003. Interaction of cytochrome *c* with cytochrome *c* oxidase: an NMR study on two soluble fragments derived from *Paracoccus denitrificans*. *Biochemistry.* 42:6005–6012.

Witt, H., F. Malatesta, F. Nicoletti, M. Brunori, and B. Ludwig. 1998a. Cytochrome-c-binding site on cytochrome oxidase in *Paracoccus denitrificans*. *Eur. J. Biochem.* 251:367–373.

Witt, H., F. Malatesta, F. Nicoletti, M. Brunori, and B. Ludwig. 1998b. Tryptophan 121 of subunit II is the electron entry site to cytochrome-c oxidase in *Paracoccus denitrificans*. *J. Biol. Chem.* 273:5132–5136.

Woolf, T. B., and B. Roux. 1994. Molecular dynamics simulation of the gramicidin channel in a phospholipid bilayer. *Proc. Natl. Acad. Sci. USA.* 91:11631–11635.

Woolf, T. B., and B. Roux. 1996. Structure, energetics, and dynamics of lipid-protein interactions: a molecular dynamics study of the gramicidin A channel in a DMPC bilayer. *Proteins.* 24:92–114.